

Article

Resonant Excitation of the Ferroelectric Soft Mode by a Narrow-Band THz Pulse

Kirill Brekhov¹, Vladislav Bilyk^{2*}, Andrey Ovchinnikov³, Oleg Chefonov³, Vladimir Mukhortov⁴ and Elena Mishina¹

¹ MIREA — Russian Technological University

² Radboud University Nijmegen

³ Joint Institute for High Temperatures of Russian Academy of Sciences (JIHT)

⁴ Southern Scientific Center of Russian Academy of Sciences

* Correspondence: vladislav.bilyk@ru.nl

Abstract: This study investigates the impact of narrow-band terahertz pulses on the ferroelectric order parameter in $\text{Ba}_{0.8}\text{Sr}_{0.2}\text{TiO}_3$ films on various substrates. The 375 nm thick BST film on an MgO (001) substrate exhibits enhanced THz-induced second harmonic generation when excited by THz pulses with a central frequency of 1.6 THz, due to the resonant excitation of the soft phonon mode. Conversely, the BST film on a Si (001) substrate shows no enhancement, due to its polycrystalline state. The 800 nm thick BST film on an MgO (111) substrate demonstrates maximum of second harmonic generation signal when excited by THz pulses at 1.8 THz, that is also very close to its soft mode frequency (1.9 THz). Notably, the frequency spectrum of the BST/MgO (111) film reveals peaks at both the fundamental and doubled frequencies, highlighting the quadratic dependence of SHG intensity on the THz pulse's electric field strength.

Keywords: THz excitation; ferroelectric; second harmonic generation

1. Introduction

Today, an important task is to develop methods for ultrafast control of the ferroelectric order parameter. Solving this problem will allow to create the new energy efficient optoelectronic devices such as memory cells and modulators [1–4]. In magnetic materials, this problem has already been solved using optical [5,6] or terahertz [7–9] pulses. However, in the case of ferroelectrics, this problem remains unsolved, since the mechanisms that allow to achieve ultrafast switching remain unclear [10–13].

At present, there are some theoretical [14–18] and experimental works that show the possibility of influencing the ferroelectric order parameter by optical [19–21] or THz [22–25] pulses. However, full and stable ultrafast polarization switching has not been demonstrated. The state of polarization in a ferroelectric is directly related to the soft phonon mode. In previous studies, broadband THz pulses have been used for ultrafast switching of ferroelectric materials. However, the result was not achieved. Therefore, we decided to try narrow-band THz pulses for direct resonant excitation of the soft phonon mode and thus influence the ferroelectric order parameter.

One of the promising materials for this is $\text{B}_{0.8}\text{Sr}_{0.2}\text{TiO}_3$ (BST). It is radiation resistant, energy efficient, as well as has fast switching time and stable parameters in a wide temperature range, and low dielectric loss [26]. BST is uniaxial ferroelectric with perovskite structure. At room temperature BST is in ferroelectric phase with tetragonal unit cell (space group $P4mm$) and goes to paraelectric phase with a cubic unit cell (space group $Pm3m$) above the Curie temperature. For the study, we chose BST films on two types of substrates with different orientations: MgO(001), MgO(111) and Si(001).

Magnesium oxide was chosen because is a typical substrate material for BST films and other perovskite-like ferroelectrics, since they have fairly close cell parameters, and there is a well-established deposition technology, which makes it possible to obtain high-quality films. Silicon was chosen because the integration of ferroelectric films into silicon technology is currently a topical issue

[27]. The use of ferroelectrics as a gate in a field-effect transistor makes it possible to create a non-volatile and electrically reprogrammable memory cells [28]. It should be noted that ferroelectric materials are deposited on silicon substrates at high temperatures. This leads to the mutual diffusion of the components at the ferroelectric-semiconductor interface, the formation of a transition layer, and deterioration of the crystal structure [29]. As a result, instability of the polarized state occurs and the number of rewriting cycles is reduced. To solve these problems, transition layers based on simple oxides such as $(\text{Ba,Sr})\text{TiO}_3$ [30,31] with a thickness of several nanometers are formed at the interface between the semiconductor and the ferroelectric [32]. In addition, depositing BST on silicon when creating solar cells enables more efficient absorption of visible and ultraviolet radiation [33,34], which significantly increases their efficiency.

Here we present the investigations results of the strong narrow-band THz pulses effect on ferroelectric soft mode at $\text{B}_{0.8}\text{Sr}_{0.2}\text{TiO}_3$ films deposited on $\text{MgO}(001)$, $\text{MgO}(111)$ and $\text{Si}(001)$ substrates.

2. Materials and Methods

We investigated the nonlinear optical response dynamics in three barium-strontium titanate ($\text{B}_{0.8}\text{Sr}_{0.2}\text{TiO}_3$, BST) films under excitation by narrow-band THz pulses of few picoseconds duration. These samples were fabricated by radio-frequency (RF) sputtering of a $\text{B}_{0.8}\text{Sr}_{0.2}\text{TiO}_3$ ceramic target. The first sample was a 375 nm thick BST film deposited on a (001)-oriented MgO substrate. The second sample had the same thickness and composition, but with a sublayer of the same film with a thickness of 2.5 nm and deposited on a silicon substrate. The substrate was the monocrystalline p-type silicon with a resistivity of 12 Ohm/cm and crystallographic orientation (001) [34]. The third sample was an 800 nm thick BST film on a (111)-oriented MgO substrate. The sample fabrication processes are described in more detail in [27,32,34].

The XRD patterns of BST/ $\text{MgO}(001)$, BST/ $\text{Si}(001)$ and BST/ $\text{MgO}(111)$ samples are shown in Figure 1a), 1b) and 1c), respectively.

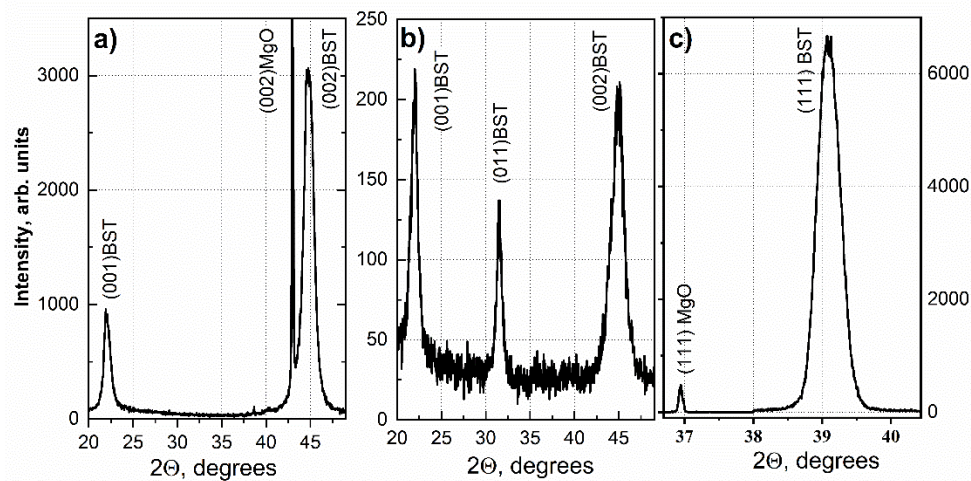


Figure 1. XRD patterns of a) BST/ $\text{MgO}(001)$, b) BST/ $\text{Si}(001)$, c) BST/ $\text{MgO}(111)$.



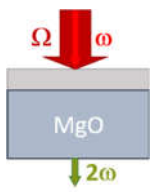
Figure 1a) shows that the 375 nm thick BST film on the $\text{MgO}(001)$ substrate is monocrystalline, with the spontaneous polarization vector directed perpendicularly to the substrate surface. The lattice parameter c for this sample is 0.4041 nm. In contrast, Figure 1b) demonstrates that the 375 nm thick BST film on the (001)-oriented silicon substrate is polycrystalline, containing crystallites with (001) and (011) plane orientations parallel to the substrate plane. The spontaneous polarization vector for (001) crystallites is perpendicular to the substrate surface, while for (011) crystallites, it is at an angle of about 45 degrees. The lattice parameter for this film is $c = 0.4035$ nm.

Figure 1c) shows that the BST film on the $\text{MgO}(111)$ substrate is epitaxial and contains only a rhombohedral phase, with polarization directed perpendicularly to the substrate. The unit cell parameters are $a = 0.39616$ nm and $\alpha = 89.519^\circ$. The XRD pattern demonstrates that the film is oriented

along the [111] direction, so $[111]_{\text{film}} \parallel [111]_{\text{MgO}}$. The unit cell volume of the rhombohedral BST film is 1.5% less than that of the tetragonal ceramic target.

It should be noted that the BST/MgO(001) film has strong stress at the film/substrate interface, significantly higher than in the BST film on the (111)MgO substrate. In the silicon film, this stress are also considerably lower due to the 2.5 nm thick BST sublayer, which inhibits mutual diffusion of the components and encourages BST crystallization in the ferroelectric phase [27].

Table 1. The samples.

	Ba _{0.8} Sr _{0.2} TiO ₃ /MgO(001)	Ba _{0.8} Sr _{0.2} TiO ₃ /Si(001)	Ba _{0.8} Sr _{0.2} TiO ₃ /MgO(111)
Crystal structure	Single crystal	Polycrystalline	Single crystal
Crystallographic orientation	(001)	(001, 011)	(111)
Thickness d, nm	375	375	800
Geometry	Transmission, 0°	Reflection, 45°	Transmission, 0°
			
Coherence length, nm	1150 nm	70 nm	1150 nm
THz field, kV/cm	700÷1400	700÷1400	320÷560

The dynamics of nonlinear optical response in BST films when they are excited by narrow-band THz pulses was investigated using a modified experimental setup described in [35].

A Cr:forsterite laser system with a wavelength of 1240 nm, a pulse repetition rate of 10 Hz, and a duration of 100 fs was used to generate narrow-band THz pulses. THz pulse generation occurred in the organic crystal OH1. To generate narrow-band THz pulses, the amplified laser pulse was split into two parts, with each passing through one arm of a Mach-Zehnder type interferometer. By adjusting the delay between these pulses before compression, it was possible to achieve beating of the optical pulses at a necessary frequency. The resulting frequency-modulated optical chirp irradiated the OH1 crystal, generating narrow-band terahertz radiation. The spectral line width was 0.1-0.2 THz, depending on the central frequency. Measurements of the temporal waveform of narrow-band THz radiation pulses were performed in the electro-optical detection scheme on a 1 mm thick ZnTe crystal [36]. Figure 2 shows (a) the temporal waveform and (b) the corresponding spectrum of narrow-band THz pulses at a frequency of 1.2 THz.

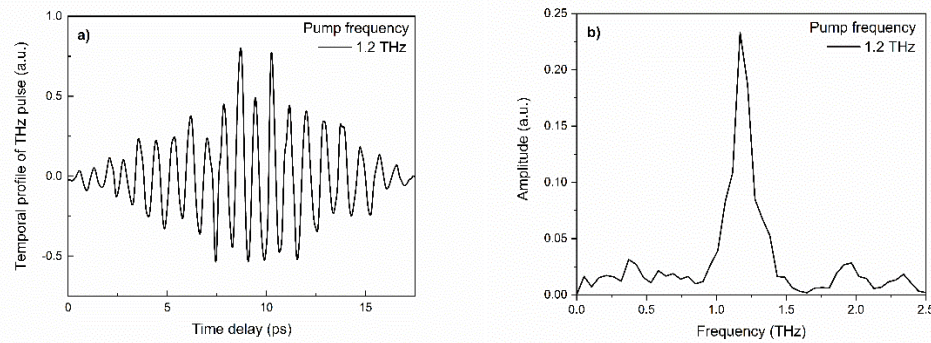


Figure 2. a) Temporal waveform and b) spectrum of narrow-band THz pulses at 1.6 THz.

Similar measurements of temporal waveforms were made in a frequency range of 1.2 to 2.0 THz. To estimate the electric field strength of THz pulses at various frequencies, we measured the energy of THz pulses and the spatial distribution of the THz beam in the focal plane of the focusing off-axis parabolic mirror. THz pulse energy measurements were made using a Golay cell, while the spatial distribution was measured with a terahertz camera. Thus, we obtained a comprehensive set of experimental data on the terahertz source parameters enabling us to estimate the electric field strength at different frequencies. The electric field ranged was estimated according to [37] as 320 kV/cm - 1.45 MV/cm, depending on the central generation frequency.

Detection occurred at the frequency of the second optical harmonic. This technique is one of the most sensitive methods to study the order parameter of ferroelectrics [38–40]. The BST films deposited on the MgO substrate were measured in transmission geometry while the film on the Si substrate was measured in reflection geometry.

Table 1 displays a comparison of the samples.

3. Results

Figure 3 (a-c) demonstrates the dependence of the normalized THz-induced second harmonic signal dynamics on the time delay between pump and probe pulses in BST/MgO (001), BST/Si (001), and BST/MgO (111) films, respectively, when the narrow-band pump pulses were in the range of 1.2 THz - 2.0 THz.

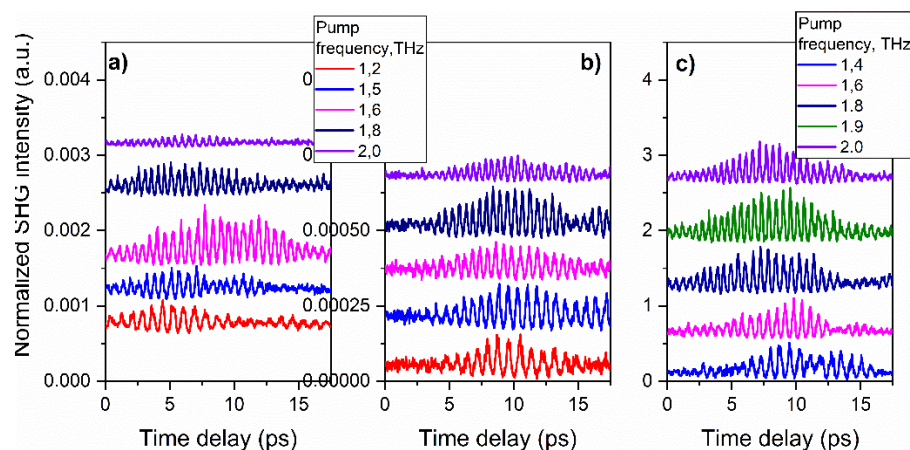


Figure 3. Dynamics of the normalized THz-induced SHG intensity for (a) BST/MgO (001), (b) BST/Si (001), (c) BST/MgO (111) at different central frequency of the excitation THz pulse. For the convenience of observation, the plots are shifted along the ordinate axis.

As can be seen from Figure 3 (a)-(c), the intensity of the THz-induced SHG signal for all three samples correlates with the temporal waveform of the excitation THz pulse, shown in Figure 1 (a). In

addition, the figure shows that for the BST/MgO (001) film, the highest SHG intensity is observed at the excitation THz pulse frequency of 1.6 THz. In Figures 3 (b) and 3 (c) it is not possible to unambiguously identify the pumping frequency that provides the highest SHG signal.

Figure 4(a)-c) demonstrates the frequency spectrums of the dependencies shown in Figure 3, obtained by the Fourier transform in the region up to 2.5 THz. For comparison, the green dashed lines represent the spectrum of the SHG signal measured when the samples are excited by broadband THz pulses with electric field up to several MV/cm [41].

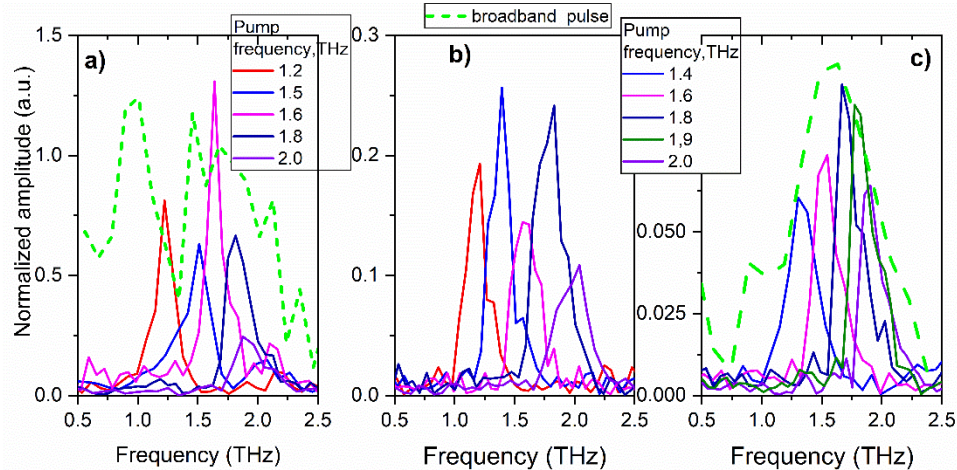


Figure 4. Frequency spectrums of the dependences presented in Figure 3 for films of (a) BST/MgO (001), (b) BST/Si (001), (c) BST/MgO (111), respectively. The green dashed line shows the SHG frequency spectrum obtained from the samples when they were excited by a broadband THz pulse.

It should be noted that, for a correct comparison, the obtained frequency dependences were successively normalized to the probe power, film thickness with regard to the coherence length, and the electric field of THz radiation. The effect of pulse propagation in the MgO substrate was also taken into account [35]. The coherence length was estimated using the expression $l_{\text{coh}} = \lambda_{\omega} / 4(n_{\omega} \pm n_{2\omega})$, where n_{ω} and $n_{2\omega}$ being the refractive indices for the fundamental and SHG waves, and + (-) refers to the reflection (transmission) geometry, respectively. Thus, for BST films on MgO substrates, the coherence length was found as 1150 nm. This value exceeds the film thickness, allowing us to use the exact sample thickness for normalization. For the BST film on Si substrate the coherence length was estimated as 70 nm. This value was used in the normalization.

Normalization on the THz field was performed relative to the first degree of its strength. This is due to the fact that in the presented frequency spectrums only the peaks corresponding to the frequency of excitation THz pulses are observed.

Figure 4(a) demonstrates that the spectral amplitude of the signal measured at the excitation pulse frequency of 1.6 THz significantly exceeds the spectral amplitudes of the signals obtained at other excitation pulse frequency. This can be explained as follows. The soft ferroelectric mode in the BST film on the MgO (001) substrate has a frequency of about 1.67 THz [22,35,42]. By exciting this material with narrow-band THz pulse of a suitable central frequency, we act on the polar ion more effectively, displacing it from the equilibrium state, thereby increasing the polarization of the medium. Since the SHG signal intensity is proportional to the second degree of the polarization, the amplification of the SHG signal at 1.6 THz shown in Figure 4(a) may be explained by the resonance effect on the polar ion.

Figure 4(b) shows that, for the BST/Si (001) film the spectral amplitudes are not significantly different, while the amplitude for the 2.0 THz pump frequency it is considerably smaller. It is important to note that in this case there is no pronounced resonance amplification of the signal. This can be explained by the fact that the sample BST/Si (001) is polycrystalline with regions with different polarization directions relative to the sample surface, which are not affected equally by excitation THz pulses.

Figure 4(c) demonstrates the frequency spectrum for the BST/MgO (111) film in the range up to 2.5 THz. It can be seen that the peak corresponding to the excitation pulse frequency of 1.8 THz has the highest intensity. This can be explained by the fact that according to work [43] the soft ferroelectric mode in $\text{Ba}_{0.8}\text{Sr}_{0.2}\text{TiO}_3$ film on MgO substrate with crystallographic orientation (111) has a frequency of about 1.9 THz. The maximum amplitude of the peak with a frequency of 1.8 THz, rather than 1.9 THz, can be explained by the width of the spectral line in this range of about 0.2 THz.

Thus, Figures 4 a) and c) demonstrate that the use of narrow-band THz pulses to excite phonon modes is much more efficient than broadband THz pulses. In particular, they make possible the resonant excitation of the soft phonon mode in ferroelectrics.

Figure 5 presents the frequency spectrums for the BST/MgO (111) film in the range from 2.2 THz to 4.5 THz. For this sample, the frequency spectrums show a second peak at double frequency of the excitation THz pulse. No second peak is observed in the frequency spectrums of the other two samples. These dependences were normalized to the second degree of the THz field strength.

The presence of two peaks in the spectrum at the fundamental and at the doubled frequency can be explained by the fact that the dependence of the SHG intensity on the external electric field is quadratic. Indeed, the SHG intensity in the THz field can be represented as a decomposition either by the THz field E_Ω in the case of a non-ferroelectric crystal:

$$I^{2\omega}(E_\Omega) \propto (\chi^{(2)} + \chi_E^{(3)} E_\Omega)^2 (I^\omega)^2, \quad (1)$$

or by polarization $P(E_\Omega)$ in the case of a ferroelectric crystal

$$I^{2\omega}(P(E_\Omega)) \propto (P_0 + \chi_P^{(3)} P(E_\Omega))^2 (I^\omega)^2, \quad (2)$$

where $\chi^{(2)}(2\omega; \omega, \omega)$ - crystallographic quadratic susceptibility, $\chi_E^{(3)}(2\omega; \Omega, \omega, \omega)$ - cubic susceptibility. The cubic susceptibility can be considered as a measure of polarization switchability: the higher the value of $\chi^{(3)}$, the lower THz field is required to control (switch) polarization.

Obviously, in the case of linear dependence of $P(E_\Omega)$, for example, in weak fields, relations (1) and (2) are identical. In the general case, in order to distinguish (1) and (2), it is necessary to investigate the dependences of the SHG intensity on the THz field.

When decomposing the second degree of the sum, two field-dependent terms appear: linear I_2 and quadratic I_3 :

$$I_2 \propto \chi^{(2)} \chi_E^{(3)} E_\Omega, \quad (3a)$$

$$I_3 \propto (\chi_E^{(3)})^2 (E_\Omega)^2. \quad (3b)$$

These terms in the Fourier decomposition give, respectively, signals at the fundamental Ω and doubled 2Ω frequencies of the incident wave.

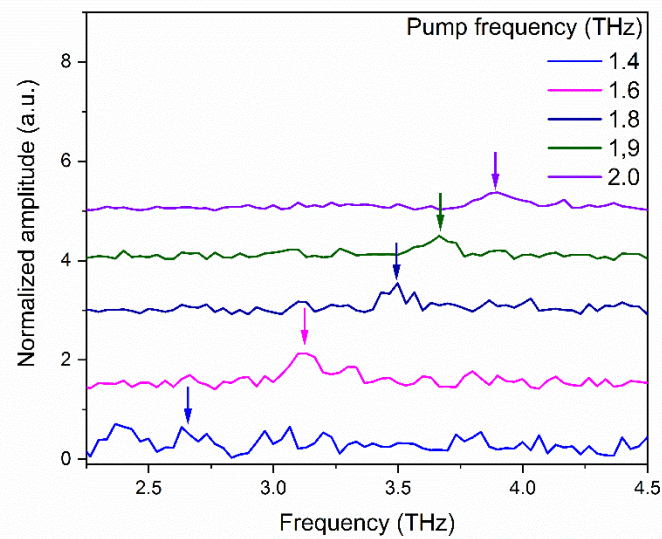


Figure 5. Frequency spectrums for the BST/MgO (111) sample in the range of 2.2-4.5 THz. The normalized amplitude on Figure 5 is three orders of magnitude less than on Figure 4.

4. Conclusions

In conclusion, we demonstrated two important issues of the developed technique. Firstly, the narrow-band THz pulse may excite the specific modes in ferroelectric, including the soft mode. This should result in a dynamical polarization switching, analogously to the case of a broadband excitation. Secondly, excitation is much stronger for frequencies close to a specific mode, which means a resonant excitation. This is in contrast to a broadband excitation, where the resonances cannot be isolated.

The developed narrow-band THz spectroscopy allows us to compare the impact of the input THz field on ferroelectric polarization measured by SHG in different samples. The highest impact or the highest switchability was achieved in 800 nm thick BST film on an MgO (111) substrate. This can be explained by the presence in this sample of polarization component parallel to the THz field. The lowest impact or the lowest switchability was obtained in 375 nm thick BST film on a Si (001) substrate. This is due to its polycrystalline structure. The single crystalline BST film on an MgO (001) substrate demonstrates intermediate impact.

Author Contributions: Conceptualization: E. Mishina; methodology: A. Ovchinnikov, O. Chefonov; software: O. Chefonov; validation, X.X., Y.Y. and Z.Z.; formal analysis: K. Brekhov; investigation K. Brekhov, V. Bilyk; sample preparation: V. Mukhortov; data curation K. Brekhov; writing—original draft preparation: K. Brekhov; writing—review and editing: E. Mishina, V. Bilyk; visualization K. Brekhov; supervision E. Mishina; project administration: E. Mishina; funding acquisition: E. Mishina.

Funding: This work was mainly supported by the Russian Science Foundation grant №20-72-10178. The work of E.D. Mishina (strategy of the research, data processing, writing the paper) was supported by Russian Science Foundation grant № 22-12-00334.

Conflicts of Interest: The authors have no conflicts of interest to declare.

References

- Kim, D.-Y.; Moon, S.E.; Kim, E.-K.; Lee, S.-J.; Choi, J.-J.; Kim, H.-E. Electro-Optic Characteristics of (001)-Oriented Ba_{0.6}Sr_{0.4}TiO₃ Thin Films. *Appl. Phys. Lett.* **2003**, *82*, 1455–1457, doi:10.1063/1.1556962.
- Mukhortov, V.M.; Masychev, S.I.; Golovko, Y.I.; Chub, A. V.; Mukhortov, V.M. Application of Nanodimensional Barium-Strontium Titanate Films in Tunable Microwave Devices. *Tech. Phys.* **2006**, *51*, 1359–1361, doi:10.1134/S1063784206100173.
- Brekhov, K.A.; Lavrov, S.D. Electro-Optic Properties of Ba_{0.8}Sr_{0.2}TiO₃ Thin Film. *Ceram. Int.* **2020**, doi:10.1016/j.ceramint.2020.09.148.
- Eltes, F.; Mai, C.; Caimi, D.; Kroh, M.; Popoff, Y.; Winzer, G.; Petousi, D.; Lischke, S.; Ortmann, J.E.; Czornomaz, L.; et al. A BaTiO₃-Based Electro-Optic Pockels Modulator Monolithically Integrated on an Advanced Silicon Photonics Platform. *J. Light. Technol.* **2019**, *37*, 1456–1462, doi:10.1109/JLT.2019.2893500.
- Stanciu, C.D.; Hansteen, F.; Kimel, A. V.; Kirilyuk, A.; Tsukamoto, A.; Itoh, A.; Rasing, T. All-Optical Magnetic Recording with Circularly Polarized Light. *Phys. Rev. Lett.* **2007**, *99*, doi:10.1103/PhysRevLett.99.047601.
- Vahaplar, K.; Kalashnikova, A.M.; Kimel, A. V.; Gerlach, S.; Hinzke, D.; Nowak, U.; Chantrell, R.; Tsukamoto, A.; Itoh, A.; Kirilyuk, A.; et al. All-Optical Magnetization Reversal by Circularly Polarized Laser Pulses: Experiment and Multiscale Modeling. *Phys. Rev. B* **2012**, *85*, 104402, doi:10.1103/PhysRevB.85.104402.
- Blank, T.G.H.; Grishunin, K.A.; Ivanov, B.A.; Mashkovich, E.A.; Afanasiev, D.; Kimel, A. V. Empowering Control of Antiferromagnets by THz-Induced Spin Coherence. **2022**.
- Blank, T.G.H.; Grishunin, K.A.; Zvezdin, K.A.; Hai, N.T.; Wu, J.C.; Su, S.-H.; Huang, J.-C.A.; Zvezdin, A.K.; Kimel, A. V. Two-Dimensional THz Spectroscopy of Nonlinear Phononics in the Topological Insulator MnBi_2Te_4 . **2022**.
- Mashkovich, E.A.; Grishunin, K.A.; Zvezdin, A.K.; Blank, T.G.H.; Zavyalov, A.G.; van Loosdrecht, P.H.M.; Kalashnikova, A.M.; Kimel, A. V. Terahertz-Driven Magnetization Dynamics of Bismuth-Substituted Yttrium Iron-Gallium Garnet Thin Film near a Compensation Point. *Phys. Rev. B* **2022**, *106*, 184425, doi:10.1103/PhysRevB.106.184425.
- Kalashnikova, A.M.; Kimel, A. V.; Pisarev, R. V.; Gridnev, V.N.; Kirilyuk, A.; Rasing, T. Impulsive Generation of Coherent Magnons by Linearly Polarized Light in the Easy-Plane Antiferromagnet FeBO₃. *Phys. Rev. Lett.* **2007**, *99*, 167205, doi:10.1103/PhysRevLett.99.167205.
- Kalashnikova, A.M.; Kimel, A. V.; Pisarev, R. V.; Gridnev, V.N.; Usachev, P.A.; Kirilyuk, A.; Rasing, T. Impulsive Excitation of Coherent Magnons and Phonons by Subpicosecond Laser Pulses in the Weak Ferromagnet FeBO₃. *Phys. Rev. B* **2008**, *78*, 104301, doi:10.1103/PhysRevB.78.104301.
- Subkhangulov, R.R.; Henriques, A.B.; Rappl, P.H.O.; Abramof, E.; Rasing, T.; Kimel, A. V. All-Optical Manipulation and Probing of the d-f Exchange Interaction in EuTe. *Sci. Rep.* **2014**, *4*, 4368, doi:10.1038/srep04368.
- Mikhaylovskiy, R.V.; Hendry, E.; Secchi, A.; Mentink, J.H.; Eckstein, M.; Wu, A.; Pisarev, R.V.; Kruglyak, V.V.; Katsnelson, M.I.; Rasing, T.; et al. Ultrafast Optical Modification of Exchange Interactions in Iron Oxides. *Nat. Commun.* **2015**, *6*, 8190, doi:10.1038/ncomms9190.
- Yukalov, V.I.; Yukalova, E.P. Ultrafast Polarization Switching in Ferroelectrics. *Phys. Rev. Res.* **2019**, *1*, 033136, doi:10.1103/PhysRevResearch.1.033136.
- Caputo, J.-G.; Kazantseva, E. V.; Maimistov, A.I. Electromagnetically Induced Switching of Ferroelectric Thin Films. *Phys. Rev. B* **2007**, *75*, 014113, doi:10.1103/PhysRevB.75.014113.
- Chen, P.; Paillard, C.; Zhao, H.J.; Íñiguez, J.; Bellaiche, L. Deterministic Control of Ferroelectric Polarization by Ultrafast Laser Pulses. *Nat. Commun.* **2022**, *13*, 2566, doi:10.1038/s41467-022-30324-5.
- Abalmasov, V.A. Ultrafast Reversal of the Ferroelectric Polarization by a Midinfrared Pulse. *Phys. Rev. B* **2020**, *101*, 014102, doi:10.1103/PhysRevB.101.014102.
- Zhilyaev, P.; Starykh, E.; Brekhov, K.; Mishina, E. Modeling of Ultrafast Polarization Switching in PbTiO₃. *Materialia* **2023**, *27*, 101681, doi:10.1016/j.mtla.2023.101681.
- Brekhov, K.A.; Grishunin, K.A.; Afanas'ev, D. V.; Semin, S. V.; Sherstyuk, N.E.; Kitaeva, G.K.; Mishina, E.D.; Rasing, T.; Kimel, A. V. Photoinduced Dynamics and Femtosecond Excitation of Phonon Modes in Ferroelectric Semiconductor Sn₂P₂S₆. *JETP Lett.* **2015**, *102*, 372–377, doi:10.1134/S0021364015180034.
- Brekhov, K.A.A.; Grishunin, K.A.A.; Afanas'ev, D.V. V.; Semin, S.V. V.; Sherstyuk, N.E.E.; Mishina, E.D.D.; Kimel, A.V. V. Optical Second Harmonic Generation and Its Photoinduced Dynamics in Ferroelectric Semiconductor Sn₂P₂S₆. *Phys. Solid State* **2018**, *60*, 31–36, doi:10.1134/S1063783418010080.

21. Brekhov, K.A.; Ilyin, N.A.; Mishina, E.D.; Prudkovskii, P.A.; Kitaeva, G.K. The Temperature Dependence of the Photoinduced Soft Mode in Sn₂P₂S₆ Crystal. *Int. J. Mod. Phys. B* **2019**, *33*, doi:10.1142/S0217979219500619.
22. Grishunin, K.A.; Ilyin, N.A.; Sherstyuk, N.E.; Mishina, E.D.; Kimel, A.; Mukhortov, V.M.; Ovchinnikov, A. V.; Chefonov, O. V.; Agranat, M.B. THz Electric Field-Induced Second Harmonic Generation in Inorganic Ferroelectric. *Sci. Rep.* **2017**, *7*, 687, doi:10.1038/s41598-017-00704-9.
23. Bilyk, V.; Mishina, E.; Sherstyuk, N.; Bush, A.; Ovchinnikov, A.; Agranat, M. Transient Polarization Reversal Using an Intense THz Pulse in Silicon-Doped Lead Germanate. *Phys. status solidi – Rapid Res. Lett.* **2021**, *15*, 2000460, doi:10.1002/pssr.202000460.
24. Mankowsky, R.; von Hoegen, A.; Först, M.; Cavalleri, A. Ultrafast Reversal of the Ferroelectric Polarization. *Phys. Rev. Lett.* **2017**, *118*, 197601, doi:10.1103/PhysRevLett.118.197601.
25. Grübel, S.; Johnson, J.A.; Beaud, P.; Dornes, C.; Ferrer, A.; Haborets, V.; Huber, L.; Huber, T.; Kohutych, A.; Kubacka, T.; et al. Ultrafast X-Ray Diffraction of a Ferroelectric Soft Mode Driven by Broadband Terahertz Pulses. *arXiv* **2016**, 1–5.
26. Shirokov, V.B.; Biryukov, S. V.; Mukhortov, V.M.; Yuzyuk, Y.I. Polarization of Thin Barium-Strontium Titanate Films by an External Electric Field. *Tech. Phys.* **2011**, *56*, 1175–1180, doi:10.1134/S106378421108024X.
27. Zinchenko, S.P.; Stryukov, D. V.; Pavlenko, A. V.; Mukhortov, V.M. The Effect of a Ba_{0.2}Sr_{0.8}TiO₃ Sublayer on the Structure and Electric Characteristics of Lead Zirconate Titanate Films on the Si(001) Substrate. *Tech. Phys. Lett.* **2020**, *46*, 1196–1199, doi:10.1134/S1063785020120159.
28. García, R.; Gonzalo, J.A. Dynamic Critical Behavior of Ferroelectric Triglycine Sulfate from Dielectric Loss Measurements. *Phys. Rev. Lett.* **1983**, *50*, 1501–1504, doi:10.1103/PhysRevLett.50.1501.
29. Vorotilov, K.A.; Sigov, A.S. Ferroelectric Memory. *Phys. Solid State* **2012**, *54*, 894–899, doi:10.1134/S1063783412050460.
30. Ngo, T.Q.; Posadas, A.B.; McDaniel, M.D.; Hu, C.; Bruley, J.; Yu, E.T.; Demkov, A.A.; Ekerdt, J.G. Epitaxial c -Axis Oriented BaTiO₃ Thin Films on SrTiO₃ -Buffered Si(001) by Atomic Layer Deposition. *Appl. Phys. Lett.* **2014**, *104*, 082910, doi:10.1063/1.4867469.
31. Vaithyanathan, V.; Lettieri, J.; Tian, W.; Sharan, A.; Vasudevarao, A.; Li, Y.L.; Kochhar, A.; Ma, H.; Levy, J.; Zschack, P.; et al. C-Axis Oriented Epitaxial BaTiO₃ Films on (001) Si. *J. Appl. Phys.* **2006**, *100*, 024108, doi:10.1063/1.2203208.
32. Anokhin, A.S.; Biryukov, S. V.; Golovko, Y.I.; Mukhortov, V.M. Structural and Electric Characteristics of Two-Layer Bi₄Ti₃O₁₂/(Ba,Sr)TiO₃ Thin Films Deposited on a Silicon Substrate by Radio-Frequency Sputtering at Increased Oxygen Pressures. *Phys. Solid State* **2019**, *61*, 139–144, doi:10.1134/S1063783419020033.
33. Sharma, S.; Tomar, M.; Puri, N.K.; Gupta, V. Ultraviolet Radiation Detection by Barium Titanate Thin Films Grown by Sol-Gel Hydrothermal Method. *Procedia Eng.* **2014**, *87*, 1172–1175, doi:10.1016/j.proeng.2014.11.375.
34. Pavlov, D.P.; Batalov, R.I.; Leontyev, A. V.; Zharkov, D.K.; Migachev, S.A.; Lunev, I. V.; Mukhortov, V.M.; Shaposhnikova, T.S.; Mamin, R.F. Investigation of the Barium Strontium Titanate Films on the Silicon Substrate. *Ferroelectrics* **2021**, *575*, 117–122, doi:10.1080/00150193.2021.1888233.
35. Grishunin, K.; Bilyk, V.; Sherstyuk, N.; Mukhortov, V.; Ovchinnikov, A.; Chefonov, O.; Agranat, M.; Mishina, E.; Kimel, A. V. Transient Second Harmonic Generation Induced by Single Cycle THz Pulses in Ba_{0.8}Sr_{0.2}TiO₃/MgO. *Sci. Rep.* **2019**, *9*, 697, doi:10.1038/s41598-018-36686-5.
36. Zainullin, F.A.; Khusyainov, D.I.; Kozintseva, M. V.; Buryakov, A.M. Polarization Analysis of THz Radiation Using a Wire Grid Polarizer and ZnTe Crystal. *Russ. Technol. J.* **2022**, *10*, 74–84, doi:10.32362/2500-316X-2022-10-3-74-84.
37. Sitnikov, D.S.; Romashevskiy, S.A.; Ovchinnikov, A. V.; Chefonov, O. V.; Savel'ev, A.B.; Agranat, M.B. Estimation of THz Field Strength by an Electro-Optic Sampling Technique Using Arbitrary Long Gating Pulses. *Laser Phys. Lett.* **2019**, *16*, 115302, doi:10.1088/1612-202X/ab4d56.
38. Mishina, E.D.; Sherstyuk, N.E.; Barskiy, D.R.; Sigov, A.S.; Golovko, Y.I.; Mukhorotov, V.M.; De Santo, M.; Rasing, T. Domain Orientation in Ultrathin (Ba,Sr)TiO₃ Films Measured by Optical Second Harmonic Generation. *J. Appl. Phys.* **2003**, *93*, 6216–6222, doi:10.1063/1.1563849.
39. Mishina, E.D. Nonlinear Optics of Ferroelectrics: Towards Nanometers and Picoseconds. *Ferroelectrics* **2005**, *314*, 57–72, doi:10.1080/00150190590926102.

40. Denev, S.A.; Lummen, T.T.A.; Barnes, E.; Kumar, A.; Gopalan, V. Probing Ferroelectrics Using Optical Second Harmonic Generation. *J. Am. Ceram. Soc.* **2011**, *94*, 2699–2727, doi:10.1111/j.1551-2916.2011.04740.x.
41. Mishina, E.; Bilyk, V.; Sherstyuk, N.; Sigov, A. Ferroelectric Switching by (Sub)-Picosecond Electromagnetic Pulse. *Ferroelectrics* **2021**, *577*, 1–12, doi:10.1080/00150193.2021.1916345.
42. Yuzyuk, Y.I.; Zakharchenko, I.N.; Alyoshin, V.A.; Leont'ev, I.N.; Rabkin, L.M.; Mukhortov, V.M.; Simon, P. Influence of the Growth Mechanism and Thermoelastic Stresses on the Lattice Dynamics of Heteroepitaxial Films of Barium Strontium Titanate. *Phys. Solid State* **2007**, *49*, 1759–1765, doi:10.1134/S1063783407090247.
43. Anokhin, A.S.; Yuzyuk, Y.I.; Lyanguzov, N. V.; Razumnaya, A.G.; Stryukov, D. V.; Bunina, O.A.; Golovko, Y.I.; Shirokov, V.B.; Mukhortov, V.M.; El Marssi, M. Direct Transition from the Rhombohedral Ferroelectric to the Paraelectric Phase in a (Ba,Sr)TiO₃ Thin Film on a (111)MgO Substrate. *EPL (Europhysics Lett.)* **2015**, *112*, 47001, doi:10.1209/0295-5075/112/47001.